SLAC-PUB-14340

#BU11176

Electronic structure and Magnetic Properties of Epitaxial FeRh(001) ultra-thin films on W(100)

J.-S. Lee,[1] E. Vescovo,[1] L. Plucinski,[2] C. M. Schneider,[2] and C.-C. Kao[1,*]

[1]*National Synchrotron Light Source, Brookhaven National Laboratory, Upton, New York 11973, USA*

[2]*Institute of Solid State Research IFF-9, Research Centre Jülich, Jülich, Germany*

(Dated: November 9, 2010)

Abstract

Epitaxial FeRh(100) films (CsCl structure, $\sim$ 10 ML thick), prepared *in-situ* on a W(100) single crystal substrate, have been investigated via valence band and core level photoemission. The presence of the temperature-induced, first-order, antiferromagnetic to ferromagnetic (AF$\rightarrow$ FM) transition in these films has been verified via linear dichroism in photoemission from the Fe 3p levels. Core level spectra indicate a large moment on the Fe atom, practically unchanged in the FM and AF phases. Judging from the valence band spectra, the metamagnetic transition takes place without substantial modification of the electronic structure. In the FM phase, the spin-resolved spectra compare satisfactorily to the calculated spin-polarized bulk band structure.

PACS numbers: 73.20.-r,73.20.At,75.20.En,75.70.-i

Work supported in part by US Department of Energy contract DE-AC02-76SF00515.

SLAC National Accelerator Laboratory, Menlo Park, CA 94025

I. INTRODUCTION

Stoichiometric 50:50 FeRh alloy has been studied extensively for many years. Fallot[1] reported on the discovery of an AF $\rightarrow$ FM transition in this material more than half a century ago. The unusual occurrence of a metamagnetic transition attracted considerable attention and many valuable information have been gathered over the years.

Equiatomic FeRh crystallizes in the CsCl structure. The magnetic transition happens abruptly as a function of temperature (first order transition, $T_{AF \rightarrow FM} \sim 350\ K$). The critical temperature is strongly dependent on the stoichiometry (the transition exists only within ~ 5 % deviation from the equiatomic composition) as well as on the presence of transition metals (TM) impurities. The transition is isostructural, but accompanied by a rather large lattice constant increase.[2] The transition can also be reversed by application of external pressure.[3,4] Other physical quantities undergoing large variations at the transition are thermal capacity, electrical resistivity and entropy.[5]

Magnetically, the antiferromagnetic phase has been identified via neutron scattering as of type II (AF-II), with nearest-neighbor Fe sites ordered antiferromagnetically in the (001)-planes and ferromagnetically in (111)-planes.[6] Neutron data also provide evidence of an enhanced Fe magnetic moment in this compound ($\sim 3\ \mu_B$) compared to bulk Fe metal ($\sim 2.2\ \mu_B$). According to electronic structure calculations, enhanced Fe moments are present in both the AF and FM phases. The Rh atoms are usually assumed to be unpolarized in the antiferromagnetic phase and to acquire $\sim 1\ \mu_B$ in the ferromagnetic phase.

Several models have been proposed to account for the properties of the metamagnetic transition, but the debate is still active. Early models, focusing on the conspicuous lattice expansion, attempted to justify the transition in terms of an underlying lattice instability. These theories encounter serious difficulties in explaining the large entropy jump associated with the transition. On the other side, the large variation of thermal and electrical conductivities motivated the search for an electronic origin for the change in entropy. This search generally led to theoretical models attributing a major role to modifications of the electronic structures (i.e. change in density of states, DOS) in the AF and FM phases.

Recently, interest in the FeRh system has revived. Its peculiar thermo-magnetic properties promise the realization of efficient thermally assisted magnetic recording media.[7–9] With this new interest, the metamagnetic transition has been re-scrutinized using modern

experimental techniques. Notably, time-resolved investigations have attempted to elucidate the role played by the spin-lattice dynamics in the transition.[10,11]

In spite of the richness of information on the properties of FeRh, direct spectroscopic information on this system is conspicuously scarce, especially for ultra-thin films. X-ray magnetic dichroism studies[12,13] from polycrystalline samples focused on the magnetic properties without examining effects in the electronic structure, aside from the XMCD signal in the FM phase.

In this work, we report on a comprehensive photoemission study of FeRh ultrathin films with close-to-equiatomic compositions. Epitaxial FeRh(001) films are obtained by room-temperature codeposition on a W(100) single crystal substrata, followed by mild annealing. The atomic reordering process, induced by post-annealing, is accompanied by substantial modifications of the electronic structure, apparent in core levels as well as in the valence band spectra. The appearance of a cubic LEED pattern at this stage signals the formation of a well-defined, single crystalline alloy films. The temperature dependence of the magnetic properties are monitored using magnetic linear dichroism (MLD) in the Fe $3p$ core levels. They reveal that the AF $\rightarrow$ FM metamagnetic transition, characteristic of bulk equiatomic alloy, is present also for these ultra-thin epitaxial films and in particular at their surfaces. In the ferromagnetic phase, spin-resolved valence band spectra display well polarized features which are consistent with *first-principle* calculations of the spin-polarized band structure of bulk ferromagnetic FeRh. Judging from the photoemission spectra, the metamagnetic transition is accomplished without any major change in the electronic structure. In particular, large modifications of the d-derived DOS can be excluded during the metamagnetic transition.

II. EXPERIMENTAL DETAILS

All experiments were performed at beamline U5UA at the National Synchrotron Light Source (NSLS). The beamline, equipped with a planar undulator and a high-resolution spherical-grating monochromator, is dedicated to spin-polarized angular-resolved photoemission (SP-ARPES) studies.[14]

The incident light was linearly polarized in the horizontal plane. A commercial hemispherical electron energy analyzer, coupled to a mini-Mott polarimeter for spin analysis, was

employed for these experiments. The incoming photons, incident at 45° from the sample normal, and the emitted (detected) electrons were in the horizontal plane. The emission angle was along the sample surface normal. The typical overall instrumental resolution was approximately 80 meV for spin integrated and 120 meV for spin-polarized photoemission spectra. The Sherman function of the spin-detector was estimated at 0.2. The FeRh films were magnetized along the *in-plane* [010] (vertical) direction via a pulsed current passed through a magnetizing coil placed near the sample surface. All magnetic measurements were performed in magnetic remanence.

FeRh(001) films ($\sim 10\ ML$) were grown on a W(001) single crystal at RT by coevaporation of Fe and Rh from two electron beam sources. The evaporation rate was ~ 5 Å/min. The base pressure in the chamber was 5×10^{-11} Torr and rose to about 1×10^{-10} Torr during depositions. After RT deposition, the LEED was barely visible, consisting of large, diffused spots on a high background. Annealing to 600 °C for approximately 2 *min* restored a sharp cubic LEED pattern (see Fig. 1(a)). The pattern is in registry with the underlying W(001) substrate, indicating the formation of ordered films, exposing the (001) surface. The annealing procedure has been limited because longer/higher annealing leads to substantial three dimensional island growth with partial uncovering of the substrate, as can be assessed by monitoring the W $4f$ peaks.

III. PHOTOEMISSION RESULTS AND DISCUSSION

The formation of the ordered alloy is accompanied by considerable modifications in the electronic structure, easily detected in the photoemission spectra from core levels and the valence band (see Fig. 1(b) and 1(c)).

At the 50:50 concentration the Fe $3p$ signal is more intense than Rh $4p$. This is due to a combination of favorable Fe photoemission cross sections at 130 eV ($\sigma(Fe_{3p})/\sigma(Rh_{4p}) \sim 2$) and to a Rh signal spread over a wider energy range as a consequence of the larger spin-orbit coupling in the heavier element. In the *as-grown* films, the line-shape of the Fe $3p$ is similar to metallic Fe. During the annealing process, the $3p$ spectrum broadens and shifts toward higher binding energy. These features represent the substitution of Fe nearest-neighbors with Rh atoms during the formation of the CsCl cubic structure of FeRh. The annealing process does not change appreciably the Rh-to-Fe core level intensity ratio suggesting a negligible

tendency to surface segregation, either of Fe or Rh. A more quantitative assessment cannot be safely obtained from our data due to the change in line shape of the Fe $3p$ and Rh $4p$ spectra in the alloy and in the pure metals and to their parial overlap.

The sharpening of all spectral features in the valence band spectrum upon annealing (see Fig. 1(c)) can also be partially explained by the onset of long-range crystallographic order, with the consequent decrease of inelastic scattering events for the out-going electrons. In our case, however, a more substantial charge redistribution is taking place. Consistently with the formation of the FeRh alloy at this stage, the form of the valence band is modified by the annealing process. A new peak appears close to the Fermi level and higher spectral intensity builds up at ~ 5 eV binding energy. At the relatively high photon energy used in these experiments ($E_{\rm ph} = 170$ eV), photoemission spectra represent, in first approximation, densities of states, mostly biased towards d states. The accumulation of intensity at high binding energy can be attributed to $3d$-$4d$ majority spin hybridization during alloy formation. Indeed the majority d-bands largely overlap in Fe and Rh metals. By the same mechanism, the occupied Fe minority spin states close to the Fermi level are pushed upward to become unoccupied, anti-bonding states. The result is an enhancement of the Fe magnetic moment, but also an increased separation between the Fe and Rh minority spin states. Largely unhybridized, Rh minority spin states just below the Fermi level therefore account for the sharp peak appearing in the spectra at approximately 0.5 eV binding energy.

The magnetic behavior of the FeRh films can be monitored using magnetic linear dichroism in core-level photoemission.[15] These spectra are shown in Fig. 2(a) for FeRh film in the ferromagnetic phase. The two continuous lines (black and gray) correspond to the photoemission spectra measured with up and down magnetization directions. The difference curve, the dichroism signal, is also shown. Clearly the Fe dichroism signal is much larger than the Rh one (see Fig. 2(a) inset). This is consistent with the large difference in local magnetic moments on Fe ($\sim 3\mu_B$) and Rh ($\sim 1\mu_B$) sites. The similar shape of the difference curves of the two dichroisms (within their binding energy ranges) indicates the parallel alignment of the Fe and Rh moments.

The temperature dependence of the Fe $3p$ dichroism is shown in Fig. 2(b) (bottom) in the range $100 - 600$ K. We note that a pulsed magnetic field before each series of measurements as a function of temperature was applied. It is clear that the $AF \rightarrow FM$ transition is present in the ultrathin films prepared in this study. The critical temperature of the metamagnetic

transition, separating the antiferromagnetic state (low temperature, no dichroism) from the ferromagnetic state (high temperature, finite dichroism), is $\sim$ 50K above room temperature. The main features of the transitions — e.g. the critical temperature and range of hysteretic behavior[16] — are remarkably close to the values found in bulk FeRh alloys. Only the steepness of the transition increases in the single-crystalline films; possibly an indication of the intrinsic first order nature of the transition.

It is relevant to recall that photoemission at the excitation energies used in our experiments probes at most the first few monolayers of material. These results therefore demonstrate that the metamagnetic transition is present also at the FeRh surface. Furthermore, considering the lattice strain usually associated with epitaxial thin films – particularly at their surfaces and interfaces – these observations suggests that a lattice instability is a consequence rather than the driving force of the transition.

Above the metamagnetic transition, further increasing the temperature, the magnetic signal diminishes. The Curie temperature, above which the system is paramagnetic, is at approximately 530K. It is interesting to note that at $\sim$ 430K the slope of the Curie curve appears to change slightly, accelerating the decay of the magnetization. This behavior, if further confirmed via a more direct probe of the magnetization, could indicate the disappearance of the local Rh moment via a high- to low-spin state transition. The existence of these two states for the Rh atoms has been suggested in a recent model proposed to explain the FeRh thermomagnetic behavior.[17]

The effect of the AF$\rightarrow$FM transition on the electronic structure is shown in Fig. 3. The photoemission spectra from films in the antiferromagnetic state (continuous lines, $\sim$ 100 K) and in the ferromagnetic state (open circles, $\sim$ 380 K) are superimposed to facilitate the comparison. The magnetic transition has remarkably little effect on all photoemission spectra; core levels (s-levels, top; p-levels, middle) as well as valence band (bottom). The small differences in the spectra are mostly attributable to thermal broadening.

In Fig. 3(a), the 3s and 4s spectra of Fe and Rh metals are compared to the FeRh one. The overall shift of these levels ($\sim$0.5 eV) reflects an increased local electrostatic potential in the alloy. Furthermore, the distance between the main peak and the higher energy satellite of Fe 3s increases from 4.5 eV in the metal to 5.1 eV in the alloy. Due to the absence of orbital contributions in the s-levels, the distance between the main peak and the higher energy satellite is proportional to the local spin moment on the Fe site.[18] This observation

therefore implies a larger Fe magnetic moment in the alloy.

The shape of the Fe 3s core level remains essentially unchanged during the metamagnetic transition. A larger magnetic moment is therefore present in both phases of the alloy. These observations agree with calculations of the electronic structure which give a Fe magnetic moment of approximately $3\mu_B$ in FeRh to be compared with $2.2\mu_B$ of Fe metal. Unfortunately, the signal from the Rh 4s level is too weak to permit an unambiguous assessment on the presence of a high energy satellite, as would be expected during the formation of a Rh magnetic moment in the FM state. Similarly, as in the case of the s-levels, the p-levels (Fig. 3(b)) are also mostly unaffected by the metamagnetic transition.

The angular resolved photoemission spectra from the valence band are shown in Fig. 3(c). The spectra are measured in normal emission (i.e. $\mathbf{k}_{\|} = 0$) from the (100) surface, and probe states along the bulk Δ line. The two photon energies shown sample widely spaced regions of the Brillouin zone (BZ). Assuming a free electron final state, 63 and 35 eV photon energies correspond to states close to the Γ-point and X-point, respectively. Similarly to the core levels, the valence band remains largely unchanged during the metamagnetic transition. Again the major effect is thermal broadening, easily visible at the Fermi level. This behavior is not limited to the two photon energies shown; we have explored the photon energy range between 20 to 80 eV and found essentially the same result.

The spin-polarized electronic structure in the FM phase can be examined with spin-resolved photoemission. The spin-resolved valence band spectra, measured under the same conditions as Fig. 3(c) are shown in Fig. 4. These well polarized spectra are quite complex, displaying several overlapping features in both minority and majority spin channels.

As a first step in interpreting these spectra, it is useful a comparison with band structure calculations. In magnetic 3d metals, however, electronic correlation have been shown to affect the photoemission spectra[19,20] and a more refined analysis would need to take them into proper account. The band structure caculation were performed using the WIEN2k package,[21] with default settings and a lattice constant a = 2.985 Å.[22]

The band structure along the high symmetry Δ-line is displayed in Fig. 5. The general form of the bands resembles a typical bcc elemental ferromagnet (e.g. Fe metal), doubly folded because of the two elements in FeRh.[23] This folding is indeed the reason why the photoemission spectra contains so many features.

Figure 5 also shows spin-resolved density of states (DOS) which was calculated with a

$21\times21\times21$ mesh in the BZ, with effective 286 k-points in the irreducible BZ, and plotted with 40 meV Gaussian broadening. The general shape of the DOS and its magnitude compare favorably with previous calculations,[22,24] with small alterations most likely related to the different computation methods used.

In the experimental geometry used, only initial states of Δ_1 or Δ_5 symmetry are dipole-allowed.[25] Their positions at the two high-symmetry points, Γ and X, are marked with arrows (up/down: majority/minority) in Fig. 4. Although the presence of several broad and overlapping features do not allow for an unambiguous assignment of all features, there is generally a good correspondence between the experimental features and calculated bands. The clearest feature is perhaps the Δ_5 sharp minority state close to the Fermi level ($\sim$0.2 eV binding energy) in the spectra at 35 eV, which is not present at 63 eV. Along the Δ-line the Δ_5 band disperses downward, being unoccupied at Γ and occupied at X (see Fig. 5). The majority counterpart of this state is located at a binding energy of ~ 2.5 eV, giving a rather large exchange splitting ($\Delta E_{ex} = 2.3$ eV, see Fig. 4).

The 3d-4d hybridization in this system results in an unusually variable exchange. Besides states with high exchange splitting, other d states have a much lower exchange. An example of this are the minority and majority states located at 1.8 and 3.2 eV, respectively; giving an exchange splitting of only 1.4 eV (see Fig. 4). It would be tempting to attribute states of high and low exchange to Fe and Rh states, respectively. This picture however is oversimplified as can be concluded from the site-projected calculations shown in Fig. 5 where bands are highlighted according to the weight on Fe-sites or on Rh-sites. The main features emerging from Fig. 5 are that majority bands are roughly equi-distributed on the Fe and Rh sites while the minority bands are split into two groups: Rh-like in the lower portion and Fe-like close to the Fermi level. This behavior stems from the different degree of hybridization of majority and minority states mentioned above. The main factor determining the charge distribution in the alloy is the energy location of the bands previous to the alloy formation rather than the spatial localization. The majority bands of Fe and Rh, largely degenerate, strongly hybridize forming delocalized states equally distributed on the Fe and Rh sites. The minority bands, hybridizing much less, remain localized, forming bonding states on the Rh sites and anti-bonding states on the Fe sites.[26] It is therefore meaningless to attribute exchange pairs to either Fe or Rh.

As mentioned in the introduction, there is a vast literature on the origin of the meta-

magnetic transition in FeRh. It is therefore worth to discuss our results in the context of previously published work.

A primary feature of our experimental work is the investigation of epitaxial films. The metamagnetic transition is accompanied by a relatively large (in the range of $\sim 0.5-1\%$)[27] and isotropic lattice expansion. Moreover, the transition temperature can be varied and the transition itself can even be suppressed by external pressure applied to FeRh samples. These observations have lead some researchers to link the transition to a lattice instability, somewhat along the lines of the Invar phenomena in FeNi.[28] It seems therefore appropriate to attempt FeRh experiments on single crystalline samples (epitaxial films) consisting of only a few monolayers ($\sim$ 10 ML in the present films). The FeRh bulk lattice constant is 2.99 Å while the W lattice parameter is 3.15 Å. The anticipated consequence of this 5% mismatch is the substantial lattice strain if pseudomorphic growth is assumed. The fact that the magnetic properties of these ultrathin films are essentially the same as those of much thicker polycrystalline films, or even bulk FeRh, is a strong indication that the lattice change may not be a decisive factor of the metamagnetic transition, but rather a consequence of it.

The considerable change in the specific heat and resistivity at the metamagnetic transition had been noticed early on in the study of FeRh.[29] These measurements are challenging and often have to rely on comparison of samples with slightly different stoichiometry. Nevertheless, these experimental results suggest profound changes in the electronic structure. Redistribution of charge could account for large changes of the electrical and thermal properties of the material undergoing the metamagnetic transition.[30,31] Indeed, early electronic structure calculations displayed a large change of the density of states across the transition.[22] However, core level, high-energy valence band (XPS), and low-energy valence band (ARPES) photoemission spectra do not show any significant differences across the transition. Although the relatively high temperature needed to reach the FM phase limits the resolution to about 200 meV, at least within this limit, large charge rearrangements can be excluded. The direct sampling of the electronic structure using photoemission therefore substantiates and extends previous findings obtained with ellipsometry measurements[32] and with positron annihilation techniques[33] on bulk samples. They also agree with modern first principle calculations of the electronic structure which find similar charge transfer from Rh to Fe in both magnetic phases as well as similar values for both majority and minority spin density of states at the Fermi energy.[24]

IV. SUMMARY

In conclusion, equiatomic FeRh(100) films (CsCl structure, $\sim 10ML$) have been epitaxially grown on W(100) by room temperature co-deposition of Fe and Rh, followed by moderate annealing. The formation of the ordered alloy is accompanied by profound modifications of the electronic structure, displayed in valence band and shallow core level photoemission spectra. The epitaxial ultra-thin films and particularly their surfaces display magnetic properties similar to bulk FeRh. The temperature-induced $AF \rightarrow FM$ transition is clearly detected via magnetic linear dichroism in photoemission. Surprisingly, the metamagnetic transition is accomplished without major changes in the electronic structure: valence band and core levels remain practically unaffected crossing the critical temperature. In the FM phase, the valence band spectra display well polarized features, in good agreement with spin-polarized band structure calculations.

ACKNOWLEDGEMENTS

The NSLS, Brookhaven National Laboratory, is supported by the U.S. DOE, Office of Science, Office of Basic Energy Sciences, under Contract DE-AC02-98CH10886.

---

* *Current address*: Stanford Synchrotron Radiation Light source, SLAC National Accelerator Laboratory, Menlo Park, CA 94025, USA

[1] M. Fallot, Ann. Phys. **10**, 291 (1938).

[2] L. Zsaldos, Phys. Stat. Sol. **20**, K25 (1967).

[3] L.I. Vinokurova, A.V. Vlasov, M. Pardavi-Horvath, Phys. Stat. Sol. (b), **78**, 553 (1976).

[4] N.I. Kulikov, E.T. Kulatov, L.I. Vinokurova, M. Pardavi-Horvath, J. Phys. F **12**, 91 (1992).

[5] J.S. Kouvel, J. Appl. Phys. **37**, 1257 (1966).

[6] G. Shirane, R. Nathans, and C. W. Chen, Phys. Rev. A **35**, 167 (1971).

[7] Jan-Ulrich Thiele, Stefan Maat, and Eric E. Fullerton, Appl. Phys. Lett. **82**, 2859 (2003).

[8] Jan-Ulrich Thiele, Stefan Maat, J. Lee Robertson, and Eric E. Fullerton, IEEE Trans. Magn. **40**, 2537 (2004).

[9] K. Yu. Guslienko, O. Chubykalo-Fesenko, O. Mryasov, R. Chantrell, and D. Weller, Phys. Rev B **70**, 104405 (2004).

[10] Ganping Ju, Julius Hohlfeld, Bastiaan Bergman, Rene J.M. van deVeerdonk, Oleg N. Mryasov,Jai-Young Kim, Xiaowei Wu, Dieter Weller, and Bert Koopmans, Phys. Rev. Lett. **93**, 197403 (2004).

[11] Jan-Ulrich Thiele, Matthias Buess and, Christian H. Back, Appl. Phys. Lett. **85**, 2857 (2004).

[12] C. Stamm, J.-U. Thiele, T. Kachel, I. Radu, P. Ramm, M. Kosuth, J. Minár, H. Ebert, H. A. Dürr, W. Eberhardt, and C. H. Back, Phys. Rev. B **77**, 184401 (2008).

[13] J. Chaboy, F. Bartolome, M. R. Ibarra, C. I. Marquina, and P. A. Algarabel, Phys. Rev. B **59**, 3306 (1999).

[14] E. Vescovo, H.-J. Kim, Q.-Y. Dong, G. Nintzel, D. Carlson, S. L. Hulbert, and N. V. Smith, Synchrotron Radiation News **12**, 10 (1999).

[15] Ch. Roth, F. U. Hillebrecht, H. Rose, and E. Kisker, Phys. Rev. Lett. **70**, 3479 (1993).

[16] The hysteretic behaviorare known to be affected by structural change (a 1% unit cell volume expansion), including the stress state (J. van Driel, R. Coehoorn, G. J. Strijkers, E. Bruck, and F. R. de Boer, J. Appl. Phys. **85**, 1026 (1999).) and the sample's microstructural scale (K. Kang, A. R. Moodenbaugh, and L. H. Lewis, Appl. Phys. Lett. **90**, 153112 (2007).).

[17] M. E. Gruner, E. Hoffmann, and P. Entel, Phys. Rev. B **67**, 64415 (2003).

[18] T. Kachel, C. Carbone, and W. Gudat, Phys. Rev. B **47**, 15391 (1993).

[19] J. Sánchez-Barriga, J. Fink, V. Boni, I. Di Marco, J. Braun, J. Minár, A. Varykhalov, O. Rader, V. Bellini, F. Manghi, H. Ebert, M. I. Katsnelson, A. I. Lichtenstein, O. Eriksson, W. Eberhardt, and H. A. Dürr, Phys. Rev. Lett. **103**, 267203 (2009).

[20] J. Sánchez-Barriga, J. Minár, J. Braun, A. Varykhalov, V. Boni, I. Di Marco, O. Rader, V. Bellini, F. Manghi, H. Ebert, M. I. Katsnelson, A. I. Lichtenstein, O. Eriksson, W. Eberhardt, H. A. Dürr, and J. Fink, Phys. Rev. B **82**, 104414 (2010).

[21] P. Blaha, K. Schwarz, G. K. H. Madsen, D. Kvasnicka, and J. Luitz, *An Augmented Plane Wave + Local Orbitals Program for Calculating Crystal Properties (Karlheinz Schwarz, Techn. Universitat Wien, Austria) ISBN 3-9501031-1-2* (2000).

[22] C. Koenig, J. Phys. F **12**, 1137 (1982).

[23] The FeRh CsCl-structure can be thought as a simple bcc structure with every central atom substituted with the other element. In first approximation, the resulting band structure is

therefore the one of a bcc crystal with an average electrostatic potential between Fe and Rh. The doubling of the lattice periodicity, due to the different elements, additionally results in folding the bands in reciprocal space.

[24] V.L. Moruzzi and P.M. Marcus, Phys. Rev. B **46**, 2864 (1992).

[25] A. M. Turner, A. W. Donoho, and J. L. Erskine, Phys. Rev. B **29**, 2986 (1983).

[26] The behavior shown in Fig. 5 along the Δ-line is confirmed along all high-symmetry lines of the Brillouin zone.

[27] J. S. Kouvel and C. C. Hartelius, J. Appl. Phys. **33**, 1343 (1962).

[28] W. Pepperhoff and M. Acet, *Constitution and Magnetism of Iron and its Alloys*, Springer (2001).

[29] J. Ivarsson, G.R. Pickett and J. Toth, Phys. Lett. A **35**, 167 (1971).

[30] N.V. Baranov, E.A. Barabanova, J. Alloys and Compounds **219**, 139 (1995).

[31] M. P. Annaorazov, S. A. Nikitin, A. L. Tyurin, K. A. Asatryan, and A. Kh. Dovletov, J. Appl. Phys. **79**, 1689 (1995).

[32] Liang-Yao Chen and David W. Lynch Phys. Rev. B **37**, 10503 (1988).

[33] A. Adam L. Cser, Z.S. Kajcsos, and G. Zimmer, Phys. Stat. Sol. B **49**, K79 (1972).

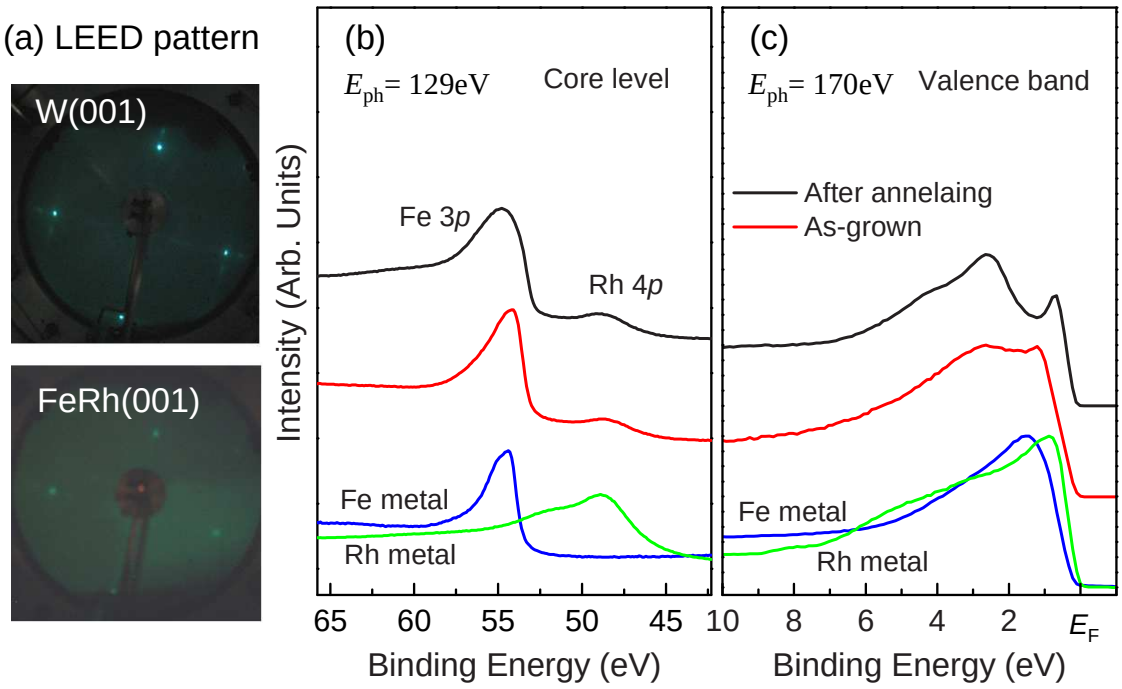

FIG. 1: (color online) (a) LEED patterns from W(001) (top, $E_{\rm ph} = 54$ eV) and from an epitaxial film (10 ML) of FeRh(001) (bottom; $E_{\rm ph} = 57.2$ eV). (b) Photoemission spectra from shallow core levels (Fe 3p and Rh 4p) from equiatomic FeRh films, before and after annealing. The spectra from films of Fe and Rh metals are also shown for comparison. (c) Valence band spectra corresponding to the spectra shown in (b).

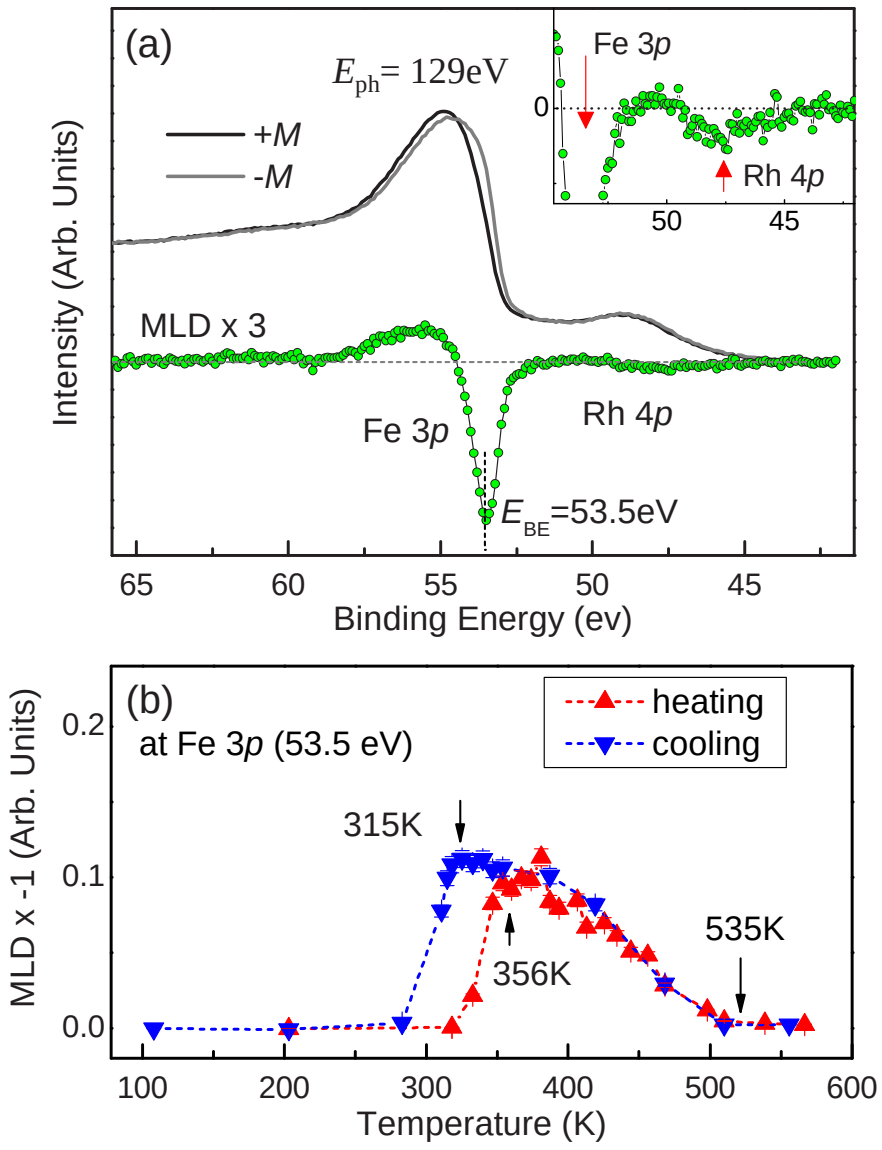

FIG. 2: (color online) (a) linear magnetic dichroism in photoemission from Fe 3p and Rh 4p core levels of an FeRh film in the ferromagnetic phase. Inset shows a blow up of the Rh 4p region. (b) temperature dependence of the Fe 3p dichroism signal.

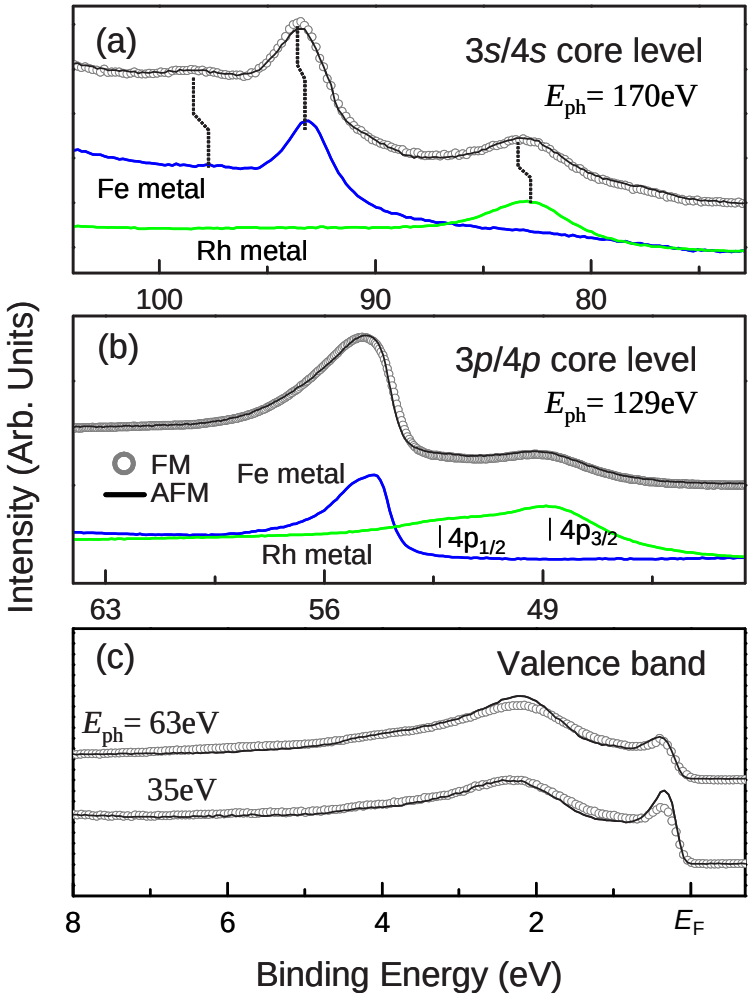

FIG. 3: (color online) (a) Fe 3s and Rh 4s core level spectra from Fe and Rh metals and from equiatomic FeRh alloy in the AF (solid line) and FM (open circles) phases; (b) similar to (a) but for Fe 3p and Rh 4p levels; (c) normal emission valence band spectra taken close to the high-symmetry Γ and X point.

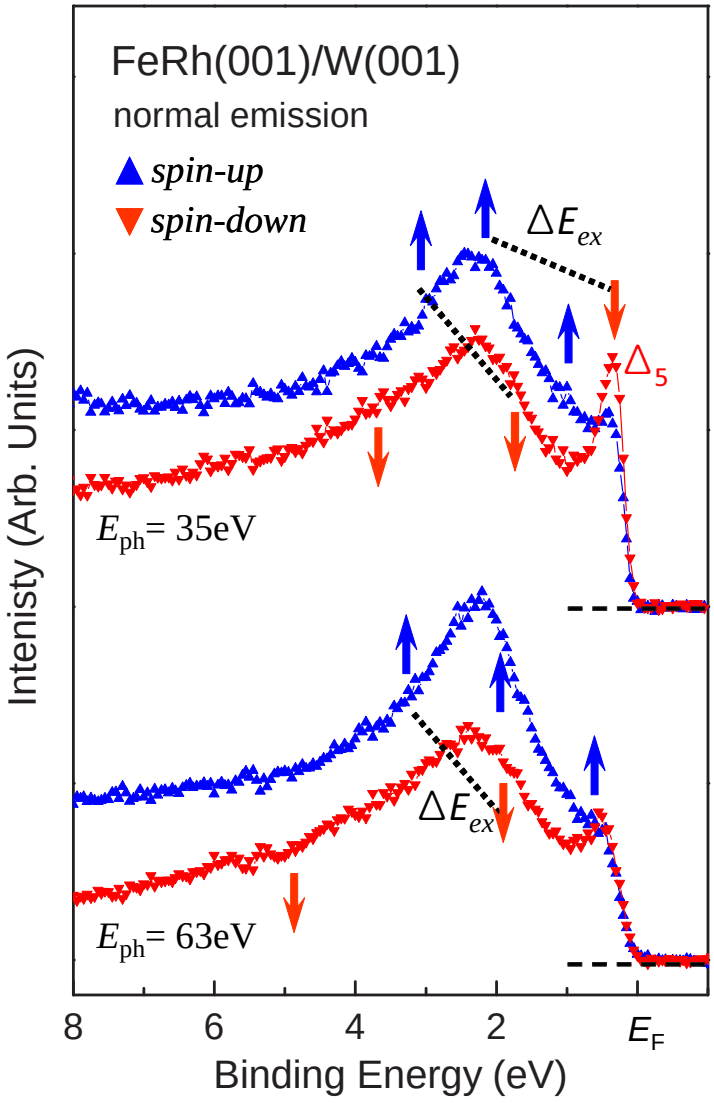

FIG. 4: (color online) Valence-band spin-resolved spectra in the ferromagnetic phase at the high-symmetry Γ and X points that are marked with arrows (up/down: majority/minority). The exchange splitting (ΔE_{ex}) is estimated to be around 1.4 eV. See text for details. The clearest feature is perhaps the Δ_5 sharp minority state close to the Fermi level ($\sim$ 0.2 eV binding energy) in the spectra.

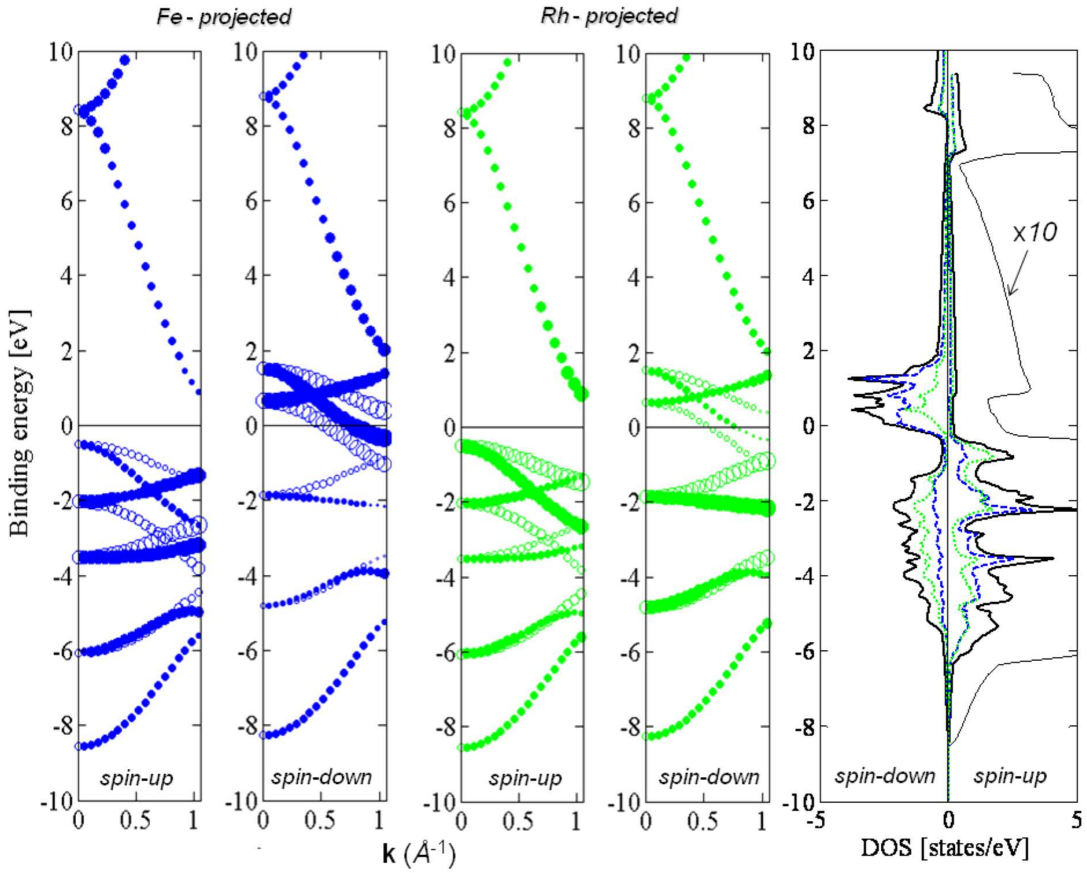

FIG. 5: (color online) Electronic bands and DOS of ferromagnetic FeRh. Only bands along the Δ high-symmetry line (Γ-X line) of the fcc BZ are shown, full circles indicate bands of Δ_1 or Δ_5 symmetries. See text for details.